Journal of Magnetism and Magnetic Materials 597 (2024) 172024

Contents lists available at ScienceDirect

Journal of Magnetism and Magnetic Materials

journal homepage: www.elsevier.com/locate/jmmm

# Coercivity enhancement in hematite/permalloy heterostructures across the Morin transition

Tianxing D. Wang [a,b,*], Ali C. Basaran [a], Ralph El Hage [a], Junjie Li [a,b], Henry Navarro [a], Felipe E. Torres [a,c], Oscar R. de la Fuente [d], Ivan K. Schuller [a]

[a] Department of Physics, Center for Advanced Nanoscience, University of California, San Diego 92093, USA
[b] Materials Science and Engineering Program, University of California–San Diego, La Jolla, CA 92093, USA
[c] Department of Physics, Universidad de Chile, Santiago 7800024, Chile
[d] Departamento de Física de Materiales, Universidad Complutense de Madrid, Madrid, Spain

ARTICLE INFO

*Keywords:*
Antiferromagnet
Morin transition
Coercivity Control
Hematite
Permalloy
Magnetic Thin Films
Interfacial Coupling

ABSTRACT

Interfacial effects between antiferromagnetic (AFM) and ferromagnetic (FM) materials have long been a center of magnetism studies. Aside from the exchange bias occurring at the AFM/FM interface, controlling the coercivity is another significant topic in magnetic recordings. The coercivity of FM materials is often determined through varying grain size, alloy composition, density of defects, etc., which is set during material growth and offers limited room for modification after growth. Hematite ($\alpha-Fe_2O_3$) is an AFM material that undergoes a temperature-controlled spin-flip transition, the so-called Morin transition. This transition gives an extra degree of freedom making hematite an intriguing component to study the exchange coupling when interfaced with an FM material. In this work, changes in the magnetic properties of soft magnetic permalloy ($Ni_{81}Fe_{19}$, or Py) thin films grown on hematite were studied across the Morin transition. Surprisingly, these samples showed a remarkable change in coercivity during the Morin transition. We attribute this effect to the magnetic domain mixture of hematite during the Morin transition. Our findings present a novel method of controlling the coercivity of plain ferromagnetic thin films.

## 1. Introduction

$\alpha-Fe_2O_3$, also known as hematite, is an antiferromagnetic (AFM) material that undergoes a spin-flip (Morin) transition at a temperature $T_M$, which is approximately 260K in bulk [1]. Below $T_M$, spins on $Fe^{3+}$ ions align parallel to the crystallographic c-axis. With increasing temperature above $T_M$, the spins reorient into the basal plane, perpendicular to the c-axis. This transition results from the single-ion anisotropy decreasing more rapidly than the magnetic dipolar anisotropy with increasing temperature, favoring an in-plane spin configuration at $T > T_M$ [2]. Above $T_M$, Dzyaloshinskii-Moriya interaction within hematite leads to spin canting, resulting in a weekly ferromagnetic order [3,4]. In hematite thin films, $T_M$ can vary between 0 to 350 K depending on multiple factors, including the presence of an external magnetic field, grain size, substrate orientation, lattice strain, pressure, and doping [1,5–12]. While hematite has been long studied, its spin-flip transition along with its tunability in $T_M$ offers hematite a unique role in spintronics. Indeed, hematite recently returned to the forefront of magnetism research thanks to the increasing interest in AFM spintronics [13–24]. Also, it has been recently proposed that hematite is an altermagnet [25].

On one hand, researchers hope to harness the ultrafast dynamics and zero net magnetization inherent to AFM in novel spintronics devices. Notably, Jani et al. and Chmiel et al. have unveiled intriguing topological features in hematite, which offers direct knowledge of the surface domain structure that holds promise for spintronics applications [13,14]. Additionally, long-range spin transport in hematite across the Morin transition was reported [15]. Moreover, hematite-based multilayers provide the means for temperature-controlled configuration of the Néel vectors. For instance, Cortie et al. observed the onset of exchange bias in nanocrystalline $\alpha-Fe_2O_3(104)/Ni_{81}Fe_{19}$ thin films when field-cooled below the blocking temperature at around 40 K [16]. Dho et al. investigated the exchange interaction in $\alpha-Fe_2O_3/Ni_{81}Fe_{19}$ thin films deposited with different crystallographic orientations, revealing the dominance of (perpendicular) spin-flop coupling in the anisotropy energy [26].

* Corresponding author at: Department of Physics, Center for Advanced Nanoscience, University of California, San Diego 92093, USA (T. D. Wang).
*E-mail address:* tiw171@ucsd.edu (T.D. Wang).

https://doi.org/10.1016/j.jmmm.2024.172024
Received 7 February 2024; Received in revised form 27 March 2024; Accepted 1 April 2024
Available online 2 April 2024

Although these examples of hematite/NiFe thin films highlight the importance of interfacial coupling, the effect of the hematite's Morin transition on the reversal and anisotropy of neighboring ferromagnetic film has not yet been studied specifically with hematite grown along [0001] crystallographic orientation. The (0001) plane in hematite is unique as it has been shown to host AFM topological features [14], and it is an uncompensated interface as opposed to $(11\bar{2}0)$ and $(1\bar{1}02)$ planes. In this work, the additional magnetic degree of freedom given by Morin transition, provides us the means to study the structural and magnetic properties of $\alpha-Fe_2O_3(0001)/Ni_{81}Fe_{19}/Pt$ thin films with different NiFe layer thicknesses ranging from 3.5 − 32 nm. Our investigation unveiled a sizable enhancement in the coercivity around $T_M$, which decreases as the temperature deviates from $T_M$. We attribute this to domain mixture in hematite across the Morin transition. This research introduces a different way to control the coercivity of a FM thin film using the Morin transition and calls for physical models to understand the underlying mechanism of this interfacial effect.

## 2. Experimental

### 2.1. Sample preparation

A 110-nm-thick $\alpha-Fe_2O_3$ thin film was deposited on $(0001)$ $Al_2O_3$ substrate using RF magnetron sputtering from a stoichiometric $Fe_2O_3$ target with ultra-high purity (99.9 %) from MSE Supplies, LLC, USA. The base pressure of the sputtering chamber was $1\times10^{-5}$Pa. Prior to the film deposition, the substrate was heated to 600 °C for 30 min for better crystalline growth and surface smoothness. The deposition was carried out in an argon/oxygen mixture with a 20 : 1 ratio and a total pressure of 0.53 Pa. The RF power supply was set to 100W, resulting in a growth rate of 0.45Å/s. After the $Fe_2O_3$ deposition, the samples were annealed in a pure oxygen environment at 700 °C for 3 h and then naturally cooled down. This annealing process relaxed stress in the films and minimized any oxygen deficiency in $Fe_2O_3$. The resulting films were confirmed to be stable under ambient conditions through structural analysis conducted over several days. NiFe films with different thicknesses were separately deposited on the grown $\alpha-Fe_2O_3$ films using a DC power source at 50 W while the substrates were maintained at 150 °C. To prevent oxidation, a 10-nm Pt capping layer was subsequently deposited on each sample. Note that all hematite layers used in this study were obtained from a single growth to ensure the AFM base has similar magnetic and surface properties.

### 2.2. Characterizations

#### 2.2.1. Structural

Fig. 1a presents the $2\theta/\omega$ X-ray diffraction (XRD) pattern of an $Al_2O_3(0001)/Fe_2O_3$ sample. The 39.08° peak corresponds to the $\alpha-Fe_2O_3$ (0006) reflection, confirming epitaxial growth. We also estimate a lower bound of crystallite size of ∼ 50 nm from the peak

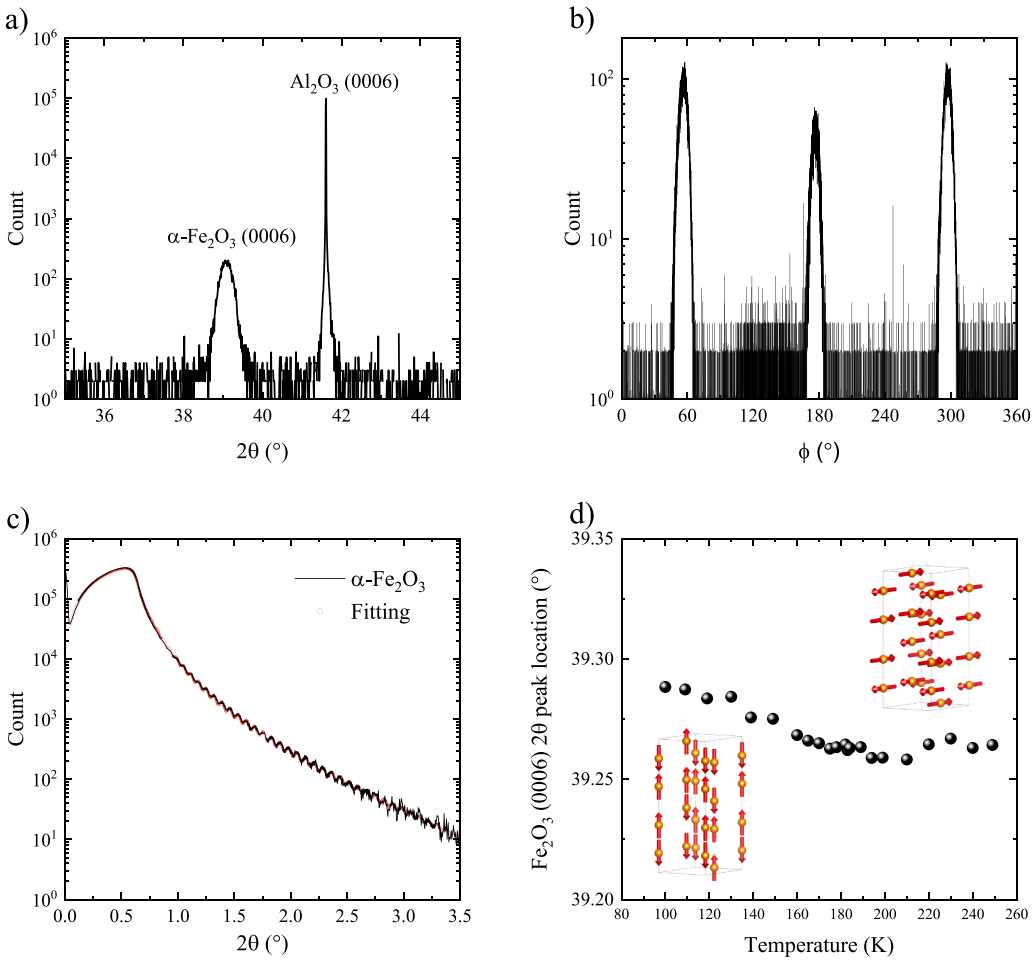


**Fig. 1.** X-ray diffraction patterns of $Al_2O_3(0001)/\alpha-Fe_2O_3$: a) $2\theta/\omega$ scan confirming the textured epitaxial growth from the $Fe_2O_3$ (0006) Bragg peak. b) Phi scan showing $(10\bar{1}0)$, $(\bar{1}110)$, $(0\bar{1}10)$ families of planes, a sixfold symmetry which matches that of the single crystal $Al_2O_3(0001)$ substrate. This suggests a good epitaxiality of the grown hematite films. c) X-ray reflectivity scan. The fitting (blue open circles) yields a thickness of 110 nm $Fe_2O_3$. d) Temperature dependence of $Fe_2O_3$ (0006) Bragg peak. The insets show the hexagonal structure of hematite and the spin configuration below and above Morin transition.

broadening using Scherrer's method [27]. In Fig. 1b, the phi-scan of the hematite (1 0 10) planes exhibits a sixfold symmetry that matches the single crystal simulation, indicating a high in-plane crystalline quality of the grown films. X-ray reflectivity data (XRR) is included in Fig. 1c. Fitting (red circles) using GenX 3 program implies a hematite layer thickness of 110 nm with a 0.3 nm surface roughness. The NiFe layer thickness was also confirmed separately using XRR data of reference samples of each NiFe deposition.

We performed $2\theta/\omega$ scans of the $Fe_2O_3$ (0006) peak as a function of temperature while heating the sample from 100 to 250 K (see Fig. 1d). Note that the grown hematite thin film exhibits a broadened Morin transition at $T_M \approx 190$ K in the heating branch, as confirmed by magnetization measurements discussed in the following section. As the temperature increases, the $2\theta$ angle of $Fe_2O_3(0006)$ first decreases monotonically which can be associated with a thermal expansion along the c-axis. Above 210 K, the decreasing trend changes, and the $2\theta$ angle of $Fe_2O_3(0006)$ increases slightly. However, the overall variation in the $2\theta$ angle of $Fe_2O_3(0006)$ for the entire temperature range is less than 0.03 °, which falls within the resolution limit of the x-ray equipment. We have not found any other studies that have reported structural phase transition or significant changes in lattice parameters accompanying the Morin transition in hematite thin films. This leads to the conclusion that structural change across the Morin transition in our grown hematite films is insignificant.

### 2.2.2. *Magnetic characterizations*

Temperature and field-dependent magnetization measurements were performed using a Quantum Design Dynacool PPMS system equipped with a VSM option. Following the deposition of hematite, the sample was subjected to a 40 kOe magnetic field annealing at 350 K for 10 min and then cooled down to 50 K while keeping a 50 Oe applied field along the basal plane of hematite. The in-plane magnetization was measured as a function of temperature in the range of 50 to 300 K with a 50 Oe magnetic field applied (Fig. 2a). As the temperature rises, the magnetization shows a sharp increase around 190 K, associated with a broad Morin transition due to the change in the magnetic order from antiferromagnetic to a weekly ferromagnetic state. Note that thin hematite films with small grain size (<100 nm) along with strain induced from substrate mismatch and structural defects can contribute to a broadened and lowered Morin transition $T_M$ compared to bulk hematite [1,5,7,9,12]. Due to the broadening of the Morin transition, we roughly define the transition temperature to be $T_M \approx 190$K, where the magnetic moment starts to increase rapidly with rising temperature.

Fig. 2b shows the $H_C$ as a function of temperature of the $\alpha-Fe_2O_3/Ni_{81}Fe_{19}(6.3nm)/Pt$ sample. Prior to the measurements, a similar field cooling process from 350 to 50 K with 1 kOe was applied. The $H_C$ values were extracted from isothermal magnetic hysteresis loops in the temperature range of 50 to 300 K. Intriguingly, $H_C$ is remarkably enhanced around $T_M = 190$ K but decreases monotonically at temperatures away from $T_M$. At its peak value, $H_C$ increases by ~ 53 % and ~ 33 % compared to that at 300 and 100 K, respectively. The $H_C$ of a pure Permalloy reference film grown on a similar $Al_2O_3(0001)$ substrate without hematite film showed no features across the Morin transition (Fig. 2b black data) in contrast to that of the permalloy grown on top of the hematite.

Fig. 3 shows the magnetization measurements for the $\alpha-Fe_2O_3/Ni_{81}Fe_{19}(6.3nm)/Pt$ sample. Fig. 3a presents the truncated hysteresis loops taken at 100, 185, and 300 K, around the reversal region. These three temperatures correspond to below, in the middle of, and above the Morin transition, respectively. In Fig. 3b, we plotted the "squareness" of the hysteresis loops as a function of temperature, which is defined as $M_R/M_S$, the ratio between remanence and saturation magnetization in a hysteresis loop. A harder axis leads to a smaller squareness value, while an easier axis results in a larger squareness value. Therefore, all the previous data indicate: i) an increase in the coercivity of Py while crossing $T_M$ and ii) a change in the Py magnetic reversal process from easy to hard as the temperature increases across the Morin transition.

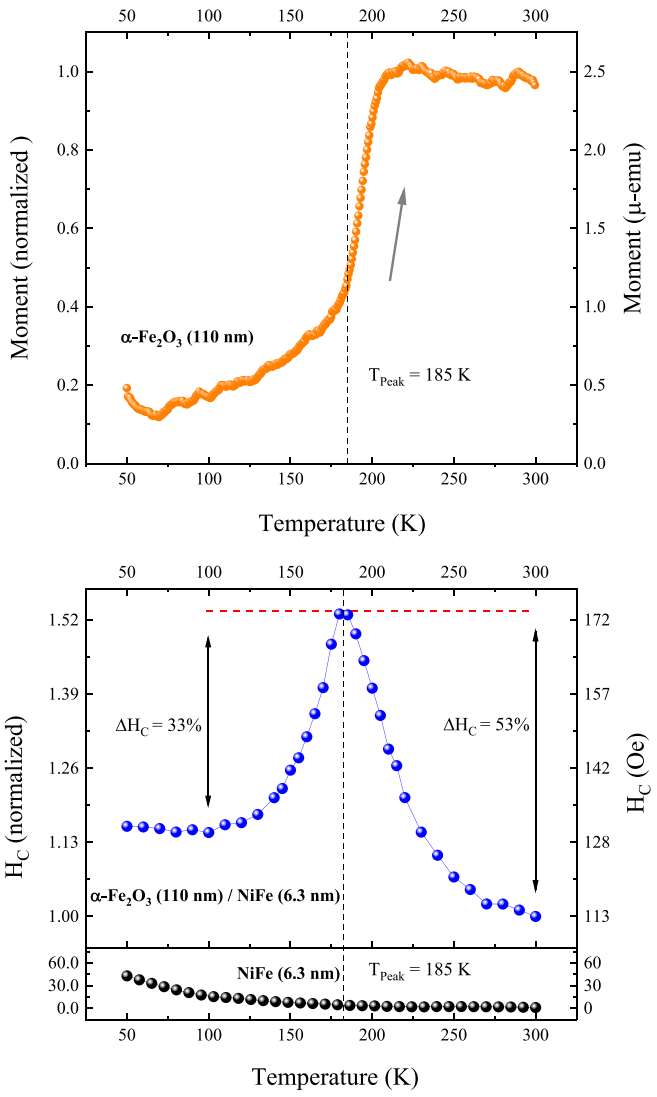


**Fig. 2.** Magnetic characterizations: a) Magnetic moment versus temperature of a 110-nm-thick $\alpha-Fe_2O_3$ film normalized to 300 K value (left y-axis). The measurement was taken when sweeping temperature from 50 to 300 K in a 50 Oe field after a 40 kOe magnetic field annealing at 350 K for 10 min and then cooled down to 50 K in a 50 Oe field. The arrow indicates the temperature sweep direction. b) Coercive field as a function of temperature for a 6.3-nm-thick Permalloy $Ni_{81}Fe_{19}$ film grown on the same hematite $\alpha-Fe_2O_3(110nm)$ film. The lower panel shows $H_C$ of a pure Permalloy layer grown on a $Al_2O_3(0001)$ substrate which is featureless across the Morin transition. $H_C$ values are obtained from the hysteresis loops at corresponding temperatures (right y-axis) and normalized to 300 K value (left y-axis). $\Delta H_C$ marks the percentage change of coercivity at 100 K and 300 K when compared to the maximum $H_C$ at 185 K. In both panels, the vertical dashed line marks the temperature $T_{peak} = 185$ K where $H_C$ reaches the maximum.

## 3. Discussion

In the $\alpha-Fe_2O_3/Ni_{81}Fe_{19}(6.3\,nm)/Pt$ sample, the most tantalizing discovery is a coercivity enhancement that reaches its maximum effect at $T_{peak} = 185$ K (Fig. 2b). When the temperature changes away from $T_{peak}$, $H_C$ resumes a monotonic decreasing trend with increasing temperature. At its peak value, $H_C$ increases by 53 % and 33 % compared to that at 300 and 100 K respectively. This coercivity enhancement is evidently correlated with the Morin transition in the $\alpha-Fe_2O_3$ layer as

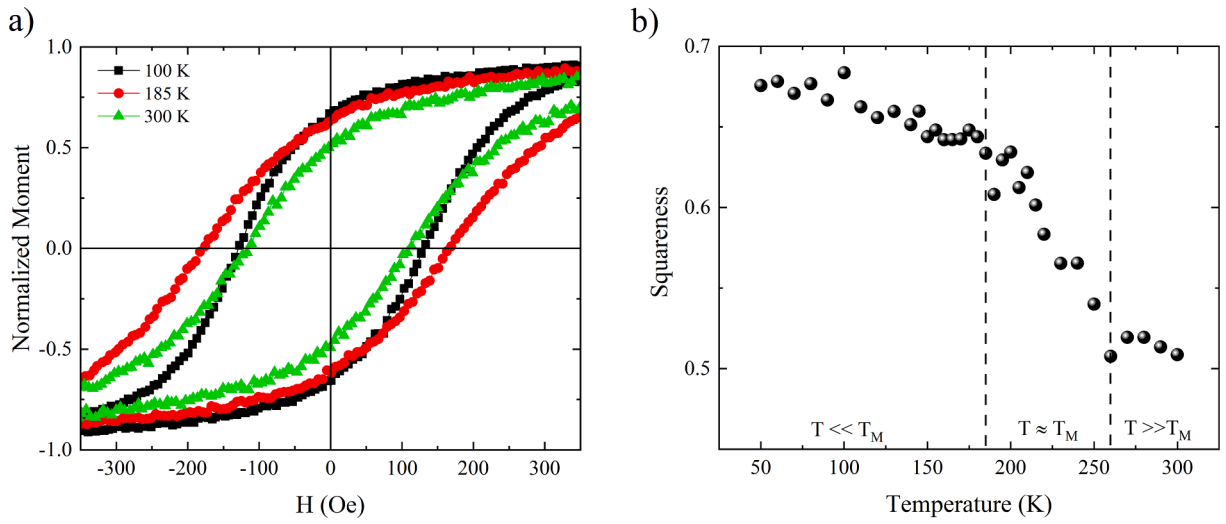


**Fig. 3.** Magnetic characterizations of $\alpha-Fe_2O_3/Ni_{81}Fe_{19}(6.3nm)/Pt$ sample: a) Truncated hysteresis loops highlighting the reversal region at below, during, and above the transition. b) Squareness (defined as $M_R/M_S$) of hysteresis loops as a function of temperature. The dashed lines separate the graph into three regions: well below, in the middle of, and well above the $T_M$.

$T_{peak}$ in $H_C$ coincides with $T_M$, which is highlighted with dashed lines in both panels in Fig. 2.

The observed $H_C$ enhancement may originate from the coexistence of two types of magnetic domains in hematite during the Morin transition. Below $T_M$ for [0001] orientation the hematite moments lie out-of-plane (OOP) due to the dominance of the single-ion anisotropy, while the Py spins tend to point in-plane (IP) due to thin film shape anisotropy. Moreover, the moment rotation during magnetization reversal in NiFe is IP, since the domain walls for the Py thin films are expected to be of the Néel type at a thickness of 6.3 nm [28]. Therefore, the AFM and FM spins are aligned perpendicularly (even during magnetization reversal) causing a weak interaction which implies a low coercivity.

As the temperature approaches $T_M$, IP domains nucleate from the otherwise OOP domains in hematite. The different IP and OOP hematite domains couple to the Py with different interactions and anisotropies. The observed Py coercivity reflects the pinning strength of the Néel domain walls during reversal. The pinning of the moving Néel wall in Py at the boundary that separates hematite IP and OOP domains is the probable reason for the coercivity enhancement. In other words, the boundaries separating the IP and OOP regions in hematite may act as pinning centers for the movement NiFe domain walls on top. Once the Morin transition is complete, NiFe is solely coupled to IP hematite domains. As a consequence, the pinning generated by the domain mixture in hematite no longer exists, leading to the decrease of the $H_C$ enhancement.

The above scenario considers solely the magnetic coupling at the interface and can explain the observed coercivity enhancement. To further evaluate this magnetically coupled interface scenario, we grew samples with different NiFe thicknesses on the same hematite and applied the same experimental protocols to compare the temperature-dependent coercive fields for each thickness (see the Supplemental Material Fig. S1). We observed coercivity enhancements (compared to room-temperature value) ranging between 35 % to 53 % for samples with thicknesses from 6.3 nm to 18.8 nm, while the peak at the transition was almost suppressed for the 32-nm-thick Py sample. The change in coercivity for the 32-nm-thick Py sample exhibited a step-like transition rather than a peak-like change around the Morin transition. This behavior may be related to the fact that above 30 nm, the domain walls change to the Bloch type [28]. In this case, the moments at the domain wall have an OOP component and the interaction with the IP moments of hematite is different from the case where all the moments of NiFe are IP.

The proposed mechanism, involving the coexistence of different coupled domains during the transition, is analogous to that of the $V_2O_3$/Ni system, where structural phase coexistence drives the $H_c$ enhancement [29]. We assessed the potential magnetoelastic coupling associated with the Morin transition in our films, and it is ruled out by the temperature-dependent X-ray measurements. The $2\theta$ angle of the $\alpha-Fe_2O_3(0006)$ XRD Bragg peak experiences a shift of less than $0.03^{\circ}$ across the Morin transition (Fig. 1d), an order of magnitude smaller compared the $0.4^{\circ}$ shift of $V_2O_3(012)$ across its structural phase transition [30]. In the $V_2O_3$/Ni system, the change in the magnetic anisotropy is induced by the structural phase transition and growth-induced strain [31]. If structural changes are associated with certain crystallographic directions, as in the case of $V_2O_3$/Ni system, an emergence of an in-plane magnetic easy axis in hematite/Py would likely be observed. However, angle-dependent ferromagnetic resonance at temperatures across the Morin transition shows no in-plane magnetic anisotropy in the hematite/permalloy heterostructures (Supplemental Material Fig. S2). This suggests that structural changes in hematite/Py heterostructures have no significant effect on the observed large $H_C$ enhancement.

Moreover, in the case of $V_2O_3$/Ni system, the squareness of the hysteresis loops remains almost identical below and above the structural phase transition of $V_2O_3$. In contrast, in our hematite/Py samples, the hysteresis squareness decreases at $T_M$ (see Fig. 3a and b), implying a change in the magnetic coupling, as discussed in the previous paragraph. Therefore, it is concluded that the $H_c$ enhancement in $\alpha-Fe_2O_3/Ni_{81}Fe_{19}(6.3\,nm)/Pt$ system arises from interfacial magnetic coupling, unlike the case of $V_2O_3$ where structural changes play a role. Controlling coercivity of an FM layer using hematite can be more controllable compared to the metal–insulator transition material of $V_2O_3$. Not only hematite is a chemically stable insulator, but also the Morin transition is highly susceptible to the application of pressure, varying grain size/shape, and doping [6,9,10,12,32]. Furthermore, hematite with magnetic phase transition is expected to be more robust compared to $V_2O_3$ with structural phase transition hence more suitable for AFM spintronics and coercivity control applications.

Additionally, we observed no in-plane anisotropy or exchange bias in our samples. The absence of in-plane anisotropy is consistent with the findings of Wittmann et al. who observed that the clamping by $Al_2O_3(0001)$ substrates led to an isotropic distribution of local Néel vectors in hematite at temperatures above $T_M$ [33]. In other words, although locally uniaxial or unidirectional anisotropy may exist in Py due to coupling to hematite, these effects are effectively averaged out

due to the isotropic distribution of Néel vectors in hematite. The loop squareness versus temperature shown in Fig. 3b supports this claim as it becomes smaller when $T > T_M$, which indicates a harder reversal caused by an isotopically distributed locally nonzero anisotropy. This observation may appear to contradict the results of Dho et al. in their $\alpha-Fe_2O_3(50nm)/Ni_{81}Fe_{19}(5nm)$ system, where they reported a clear rotation of easy axis of Py layer accompanying the Morin transition. However, the existence and rotation of the easy axis in Dho et al.'s study applies to $\alpha-Fe_2O_3$ grown on $Al_2O_3$ in $[11\bar{2}0]$ and $[1\bar{1}02]$ orientations, but not in [0001] orientation. The fact that Dho et al. did not observe the Morin transition in their 50-nm-thick $\alpha-Fe_2O_3$ grown on $Al_2O_3(0001)$ may imply that $\alpha-Fe_2O_3$ grown in [0001] orientation may be more sensitive to stress induced by substrate mismatch compared to the other growth orientations.

## 4. Conclusion

In summary, our research has revealed a sizeable coercivity enhancement around the Morin transition temperature in epitaxial $\alpha-Fe_2O_3/Ni_{81}Fe_{19}/Pt$ heterostructures deposited on $Al_2O_3(0001)$ substrate. The temperature-dependent XRD, implies that this $H_C$ enhancement is a result of magnetic rather than structural (stress) coupling. The effect is attributed to the coupling of the permalloy to a mixture of IP and OOP domains within the hematite layer across the Morin transition. Furthermore, the absence of in-plane anisotropy is in agreement with prior studies that demonstrated an isotropic domain structure in hematite grown on $Al_2O_3(0001)$, thus contributing to our understanding of the magnetic interaction between $\alpha-Fe_2O_3(0001)$ and $Ni_{81}Fe_{19}$. Our research introduces a fresh perspective on post-growth coercivity control through the Morin transition while it also calls for a detailed quantitative models to validate the proposed mechanism. The remarkable tunability of the Morin transition in $\alpha-Fe_2O_3$ opens up exciting possibilities for achieving tunable $H_C$ enhancement in such systems, paving the way for future applications in the field of AFM spintronics.

## CRediT authorship contribution statement

**Tianxing D. Wang:** Conceptualization, Data curation, Formal analysis, Project administration, Software, Visualization, Writing – original draft, Writing – review & editing. **Ali C. Basaran:** Writing – review & editing, Supervision, Methodology, Investigation, Formal analysis, Conceptualization. **Ralph El Hage:** Writing – review & editing, Methodology, Investigation. **Junjie Li:** Writing – review & editing, Methodology. **Henry Navarro:** Writing – review & editing. **Felipe E. Torres:** Writing – review & editing, Software, Investigation. **Oscar R. de la Fuente:** Writing – review & editing, Methodology, Investigation, Conceptualization. **Ivan K. Schuller:** Writing – review & editing, Supervision, Resources, Project administration, Funding acquisition, Conceptualization.

## Declaration of competing interest

The authors declare the following financial interests/personal relationships which may be considered as potential competing interests: Tianxing D. Wang reports financial support was provided by US Department of Energy Basic Energy Sciences. If there are other authors, they declare that they have no known competing financial interests or personal relationships that could have appeared to influence the work reported in this paper.

## Data availability

Data will be made available on request.

## Acknowledgements

This work is supported by the U.S. Department of Energy's Office of Basic Energy Sciences, under grant # DE-FG02-87ER45332. ORF acknowledges financial support from Ministerio de Ciencia e Innovación and Agencia Estatal de Investigación, Spain, through project PID2021–122980OB-C51, and from Ministerio de Universidades, Salvador de Madariaga program, through research stay PRX21/00740.

## Appendix A. Supplementary data

Supplementary data to this article can be found online at https://doi.org/10.1016/j.jmmm.20240.172024.

## References

[1] Ö. Özdemir, D.J. Dunlop, T.S. Berquó, "Morin transition in hematite: size dependence and thermal hysteresis", geochemistry, geophysics, Geosystems 9 (10) (2008).
[2] J.O. Artman, J.C. Murphy, S. Foner, Magnetic Anisotropy in antiferromagnetic corundum-type sesquioxides, Phys. Rev. 138 (3A) (1965) A912–A917.
[3] I. Dzyaloshinsky, A thermodynamic theory of 'weak' ferromagnetism of antiferromagnetics, J. Phys. Chem. Solid 4 (4) (1958) 241–255.
[4] T. Moriya, Anisotropic superexchange Interaction and weak ferromagnetism, Phys. Rev. 120 (1) (1960) 91–98.
[5] S. Park, H. Jang, J.Y. Kim, B.G. Park, T.Y. Koo, J.H. Park, Strain control of morin temperature in epitaxial α-Fe2O3 (0001) film, EPL 103 (2) (2013).
[6] H. Jani, J. Linghu, S. Hooda, R.V. Chopdekar, C. Li, G.J. Omar, S. Prakash, Y. Du, P. Yang, A. Banas, K. Banas, S. Ghosh, S. Ojha, G.R. Umapathy, D. Kanjilal, A. Ariando, S.J. Pennycook, E. Arenholz, P.G. Radaelli, J.M.D. Coey, Y.P. Feng, T. Venkatesan, Reversible hydrogen control of antiferromagnetic anisotropy in α-Fe2O3, Nat. Commun. 12 (1) (2021).
[7] L. Suber, P. Imperatori, A. Mari, G. Marchegiani, M.V. Mansilla, D. Fiorani, W. R. Plunkett, D. Rinaldi, C. Cannas, G. Ennas, D. Peddis, Thermal hysteresis of morin transition in hematite particles, PCCP 12 (26) (2010) 6984–6989.
[8] J. Wang, V. Aguilar, L. Li, F. gen Li, W. zhong Wang, and G. meng Zhao, Strong shape-dependence of morin transition in α-Fe2O3 single-crystalline nanostructures, Nano Res. 8 (6) (2015) 1906–1916.
[9] D. Kubániová, L. Kubíčková, T. Kmječ, K. Závěta, D. Nižňanský, P. Brázda, M. Klementová, J. Kohout, Hematite: morin temperature of nanoparticles with different size, J. Magn. Magn. Mater. 475 (2019) 611–619.
[10] R.C. Wayne, D.H. Anderson, Pressure dependence of the morin transition in the weak ferromagnet α-Fe2O3, Phys. Rev. 155 (2) (1967) 496–498.
[11] D. Schroeer, R.C. Nininger, Morin transition in α-Fe2O3 microcyrstals, Phys. Rev. Lett. 19 (11) (1967) 632–634.
[12] D. Fiorani, A.M. Testa, L. Saber, M. Angiolini, A. Montone, M. Polichetti, Size and shape effect on the canted antiferromagnetism in α-Fe2O3 particles, Nanostruct. Mater. 12 (5–8) (1999) 939–942.
[13] F.P. Chmiel, N. Waterfield Price, R.D. Johnson, A.D. Lamirand, J. Schad, G. Van Der Laan, D.T. Harris, J. Irwin, M.S. Rzchowski, C.B. Eom, P.G. Radaelli, Observation of magnetic vortex pairs at room temperature in a planar α-Fe2O3/Co heterostructure, Nat. Mater. 17 (7) (2018) 581–585.
[14] H. Jani, J.C. Lin, J. Chen, J. Harrison, F. Maccherozzi, J. Schad, S. Prakash, C. B. Eom, A. Ariando, T. Venkatesan, P.G. Radaelli, Antiferromagnetic half-skyrmions and bimerons at room temperature, Nature 590 (7844) (2021) 74–79.
[15] R. Lebrun, A. Ross, O. Gomonay, V. Baltz, U. Ebels, A.L. Barra, A. Qaiumzadeh, A. Brataas, J. Sinova, M. Kläui, Long-distance spin-transport across the morin phase transition up to room temperature in ultra-low damping single crystals of the antiferromagnet α-Fe2O3, Nat. Commun. 11 (1) (2020).
[16] D.L. Cortie, K.W. Lin, C. Shueh, H.F. Hsu, X.L. Wang, M. James, H. Fritzsche, S. Brück, F. Klose, Exchange bias in a nanocrystalline hematite/permalloy thin film investigated with polarized neutron reflectometry, Phys Rev B Condense Matter Mater Phys 86 (5) (2012).
[17] A. Hoffmann, W. Zhang, Antiferromagnets for spintronics, J. Magn. Magn. Mater. 553 (2022).
[18] A. Chanda, C.M. Hung, A.T. Duong, S. Cho, H. Srikanth, M.H. Phan, Magnetism and spin-dependent transport phenomena across verwey and morin transitions in iron oxide/Pt bilayers, J. Magn. Magn. Mater. 568 (2023).
[19] D. Xiong, Y. Jiang, K. Shi, A. Du, Y. Yao, Z. Guo, D. Zhu, K. Cao, S. Peng, W. Cai, D. Zhu, W. Zhao, Antiferromagnetic spintronics: an overview and outlook, Fundamental Research 2 (4) (2022) 522–534.
[20] J. Han, R. Cheng, L. Liu, H. Ohno, S. Fukami, Coherent antiferromagnetic spintronics, Nat. Mater. 22 (6) (2023) 684–695.
[21] X. Wang, H. Yan, X. Zhou, H. Chen, Z. Feng, P. Qin, Z. Meng, L. Liu, Z. Liu, Noncollinear $Mn_3Sn$ for antiferromagnetic spintronics, Materials Today Physics 28 (2022).
[22] Y. Cheng, J. Tang, J.J. Michel, S.K. Chong, F. Yang, R. Cheng, K.L. Wang, Unidirectional spin hall magnetoresistance in antiferromagnetic heterostructures, Phys. Rev. Lett. 130 (8) (2023).

[23] J. Fischer, M. Althammer, N. Vlietstra, H. Huebl, S.T.B. Goennenwein, R. Gross, S. Geprägs, M. Opel, Large spin hall magnetoresistance in antiferromagnetic α-Fe2O3/Pt heterostructures, Phys. Rev. Appl 13 (1) (2020).
[24] A. El Kanj, O. Gomonay, I. Boventer, P. Bortolotti, V. Cros, A. Anane, R. Lebrun, Antiferromagnetic magnon spintronic based on nonreciprocal and nondegenerated ultra-fast spin-waves in the canted antiferromagnet α-Fe2O3, Sci. Adv. 9 (32) (2023).
[25] L. Šmejkal, J. Sinova, T. Jungwirth, Emerging Research landscape of altermagnetism, Phys. Rev. X 12 (4) (2022) 040501.
[26] J. Dho, C.W. Leung, Z.H. Barber, M.G. Blamire, Controlling the exchange interaction using the spin-flip transition of antiferromagnetic spins in Ni81Fe19/α-Fe2O3, Phys Rev B Condense Matter Mater Phys 71 (18) (2005).
[27] A.L. Patterson, The scherrer formula for X-ray Particle size determination, Phys. Rev. 56 (10) (1939) 978–982.
[28] T. Trunk, M. Redjdal, A. Kákay, M.F. Ruane, F.B. Humphrey, Domain wall structure in permalloy films with decreasing thickness at the Bloch to néel transition, J. Appl. Phys. 89 (11) (2001) 7606–7608.
[29] J. De La Venta, S. Wang, T. Saerbeck, J.G. Ramírez, I. Valmianski, I.K. Schuller, Coercivity enhancement in V2O3/Ni bilayers driven by nanoscale phase coexistence, Appl. Phys. Lett. 104 (6) (2014).
[30] A.S. McLeod, E. Van Heumen, J.G. Ramirez, S. Wang, T. Saerbeck, S. Guenon, M. Goldflam, L. Anderegg, P. Kelly, A. Mueller, M.K. Liu, I.K. Schuller, D.N. Basov, Nanotextured phase coexistence in the correlated insulator V2O3, Nat. Phys. 13 (1) (2017) 80–86.
[31] C.T. Wolowiec, J.G. Ramírez, M.H. Lee, N. Ghazikhanian, N.M. Vargas, A. C. Basaran, P. Salev, I.K. Schuller, Stress-tailoring magnetic anisotropy of V2O3/Ni bilayers, Phys Rev Mater 6 (6) (2022).
[32] N. Shimomura, S.P. Pati, Y. Sato, T. Nozaki, T. Shibata, K. Mibu, M. Sahashi, Morin transition temperature in (0001)-oriented α-Fe2O3 thin film and effect of ir doping, J. Appl. Phys. 117 (17) (2015).
[33] A. Wittmann, O. Gomonay, K. Litzius, A. Kaczmarek, A.E. Kossak, D. Wolf, A. Lubk, T.N. Johnson, E.A. Tremsina, A. Churikova, F. Büttner, S. Wintz, M.A. Mawass, M. Weigand, F. Kronast, L. Scipioni, A. Shepard, T. Newhouse-Illige, J.A. Greer, G. Schütz, N.O. Birge, G.S.D. Beach, Role of substrate clamping on anisotropy and domain structure in the canted antiferromagnet α-Fe2O3, Phys. Rev. B 106 (22) (2022).